TENTH AUSTRALASIAN FLUID MECHANICS
CONFERENCE - UNIVERSITY OF MELBOURNE
11-15 DECEMBER 1989

A TURBULENT BOUNDARY LAYER AT LOW REYNOLDS NUMBER WITH ADVERSE PRESSURE GRADIENT

J.H. WATMUFF and R.V. WESTPHAL

NASA Ames Research Center,
Moffett Field, California 94035
USA

ABSTRACT

The evolution of a low Re_θ turbulent boundary layer in an adverse pressure gradient (APG) is studied for comparison with CFD simulations by P. Spalart. A short region of favorable pressure gradient (FPG) is applied first to establish a self-preserving layer which is a suitable initial condition for the simulations. The APG is then applied rapidly such that $\beta_x \approx 2$ for $Re_\theta \approx 1500$.

CFD BACKGROUND

An important feature of the numerical method of Spalart (1988) is that there is no turbulence modelling. A high non-dimensional grid density is needed which restricts the simulations to low Reynolds numbers i.e. $R_\theta < 1500$. The key assumptions are that the streamwise evolution of the flow is slow and that the straining of the turbulence by the mean-flow can be neglected. These assumptions will inevitably cause the method to breakdown in a large APG. One of the objectives of this experiment is to obtain accurate measurements for comparison with proposed APG simulations.

RELATIONSHIP BETWEEN THE EXPERIMENT AND SIMULATION

Three requirements dictate the relationship between the experiment and simulation: (1) Matched Re_θ. (2) Matched initial conditions. The simulation begins at the first station with an equilibrium boundary layer. A mildly favorable pressure gradient is used to establish a "self-preserving layer" in the experiment. This has the added advantage of allowing upstream trip effects to decay before application of the APG. (3) Accurate C_p (pressure coefficient) measurements are required as an input for the simulation. Therefore extremely low test section speeds (e.g. 4 m/s) cannot be used.

APPARATUS AND METHODS

The layer develops on a 1m wide aluminium plate forming the test-section floor of a small open-return wind tunnel. The plate is supported above an optics table which also serves as an extremely flat and rigid mounting platform for a high-speed computer controlled 3D probe traverse. A flexible ceiling is contoured to produce the pressure distribution and two plexiglass sidewalls complete the test-section.

The y-axis (normal to the wall) of the traverse is carried by the (spanwise) z-axis which is supported within the test-section by a gantry constructed of carbon-fiber composite. The y- and z- axes use linear stepping motors for positioning. Rubber strips are used to seal gaps left between the edges of the plate and the sidewalls. The gaps provide access for mounting the gantry to carriages underneath the plate. A brushless linear d.c. motor is attached to one of these carriages for positioning of the (streamwise) x-axis. The coordinate origin is defined as the centerline of the contraction exit. The size and repeatability of the measurement volume and the maximum traversing speeds are 2100 $\pm$ 0.1 mm at 2.5 m/s in the streamwise x-direction, 95 $\pm$ 0.05mm at 1m/s in the y-direction normal to the test plate and 500 $\pm$ 0.05mm at 1m/s in the spanwise z-direction. These traversing speeds are sufficient for "flying hot-wire" measurements in regions of high turbulence intensity but this capability has not been exploited yet.

A 1mm o.d. Pitot tube is used for mean velocity (U) and Preston tube skin friction coefficient (C_f) measurements. Modified Dantec normal and cross wire probes with 2.5 μm platinum filaments are used for the turbulence measurements. The included angle between the cross wire filaments is 55°. Wall distances are set using the electrical contact of a needle with the test plate. For the wires this distance is measured by focussing a telescope on the filament and its image in the wall. A high-speed 15 bit Tustin A/D converter and a microVAX II computer are used for double-buffered data acquisition. New algorithms provide high-speed on-line data processing i.e. 25K/s for single wires and 10K/s for cross wires. All averages are obtained over a minimum period of 90s.

Total computer control of tunnel speed, probe traversal and data acquisition allows all procedures to be automated. Sophisticated software enables long duration experiments to be performed continuously over several days without manual intervention. Large measurement grids can be programmed and viewed ahead of time. Redundant safety measures and error detection/recovery schemes are located at each stage throughout the code. At a higher level, hot-wire calibration drift is monitored at regular intervals and

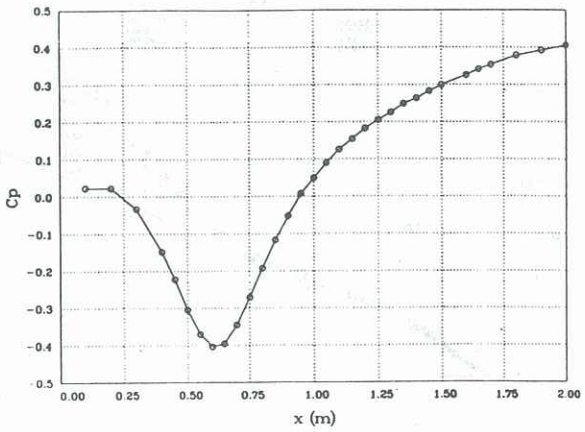

Figure 1. Variation of pressure coefficient C_p.

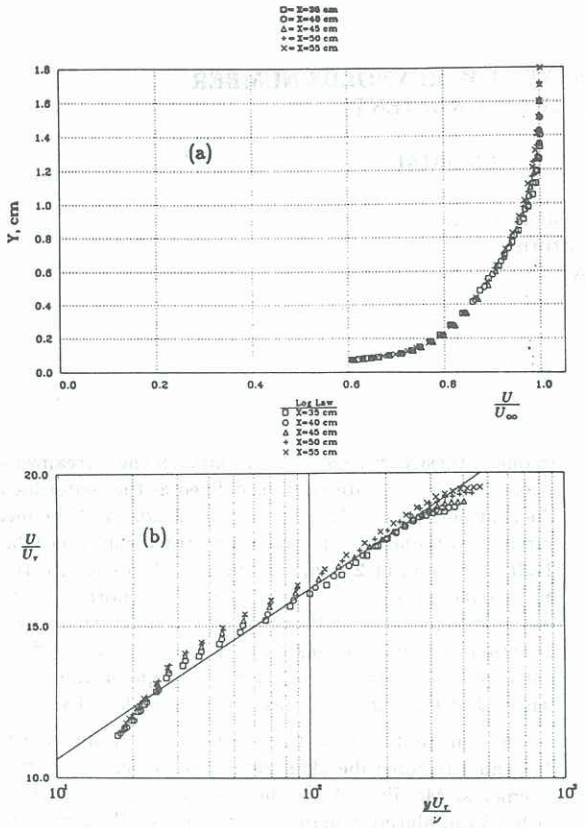

Figure 2(a) Mean velocity profiles in FPG region and (b) in wall-coordinates.

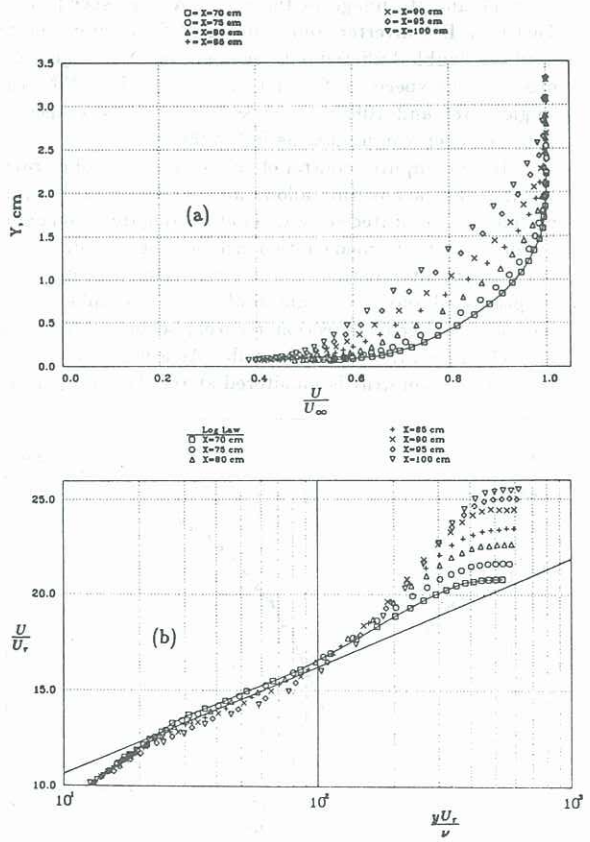

Figure 3(a) Mean velocity profiles in FPG region and (b) in wall-coordinates.

new calibrations are performed and measurements repeated (automatically) if the drift exceeds some tolerance (typically 1%).

RESULTS

Mean Flow

Selection of a transition device was performed in the absence of the PG. The incoming layers are laminar and closely follow the Blasius profile over an entrance velocity U_0 range from 6 to 12m/s. Various transition devices were tried, including 3D roughness, but a d=2.4mm wire located at x=150mm was best, producing a normal turbulent boundary by x=300mm. Figure 1 shows the pressure distribution for the experiment where U_0=6.5 m/s.

Mean-velocity profiles near the end of the FPG region in figure 2(a) indicate that the design goal of producing a self-similar sink-flow condition for compatibility with the initial conditions of Spalart's CFD simulations has been closley achieved. The shape factors $H \approx 1.47$ and the layer thicknesses (figures 4 and 5) remain fairly constant over about 20δ. High values of $C_f > 5 \times 10^{-3}$ (see figure 8) are maintained. $Re_\theta = 650$ (figure 6) at the end of the FPG and this increases the size of the APG region which can be treated by the simulations. In wall-coordinates, figure 2(b), the profiles overshoot the log law. The acceleration parameter $K = \nu/U_\infty^2(dU_\infty/dx) \approx 2 \times 10^{-6}$ and the overshoot is consistent with the CFD simulations of Spalart (1986) and the measurements of Jones and Launder (1972) in sink-flow boundary layers for comparable values of K.

Rapid application of the APG increases the growth rate and the profiles become less full resulting in large values of H and the strength of the wake component. The profiles shown in figures 3(a) and (b) cover the range of current CFD capabilities. This is a challenging flow for a simulation since at x=1m, $Re_\theta \approx 1600$ (figure 6) and $\beta_x = \frac{\delta^*}{\tau_w}\frac{dP}{dx} \approx 2$ (figure 7). C_f falls to quite low values (figure 8) but there are differences of up to 10% between the Preston tube and Clauser chart estimates. The Preston tube data is used to produce figure 3(b) and the APG

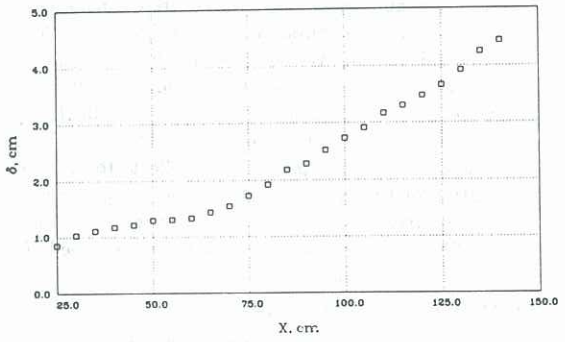

Figure 4. Variation of boundary layer thickness δ.

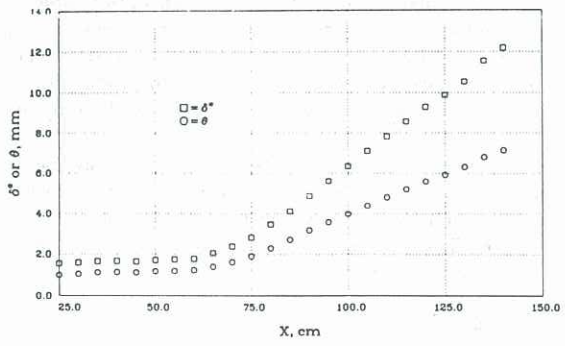

Figure 5. Displacement δ^* and momentum θ thicknesses.

is well within the limits set by Patel (1965) for his calibration. There are noticeable deviations from the log law but the data collapse closer to the wall. The deviations are consistent with the observations of Hirt and Thomann (1986) who used both a floating element and Preston tubes to measure τ_w in layers subject to strong pressure gradients. Further downstream ($x > 1m$) β_x appears nearly constant although there is considerable experimental scatter. This suggests that the layer may be approaching a new equilibrium state in this region. Better mean-flow data is required to test this conjecture.

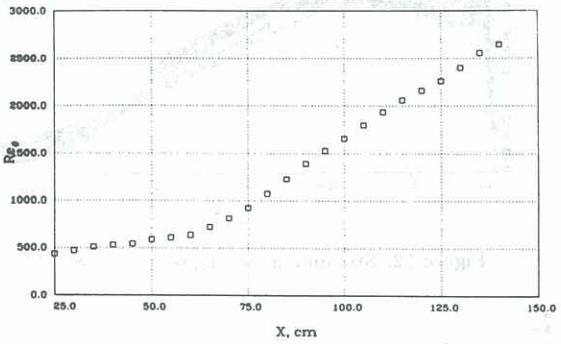

Figure 6. Variation of Re_θ with streamwise distance x.

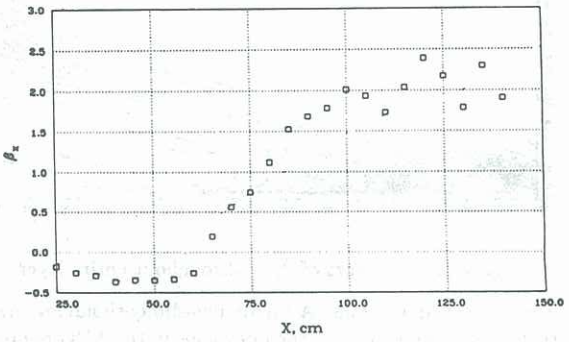

Figure 7. $\beta_x = \frac{\delta^*}{\tau_w}\frac{dP}{dx}$ with streamwise distance x.

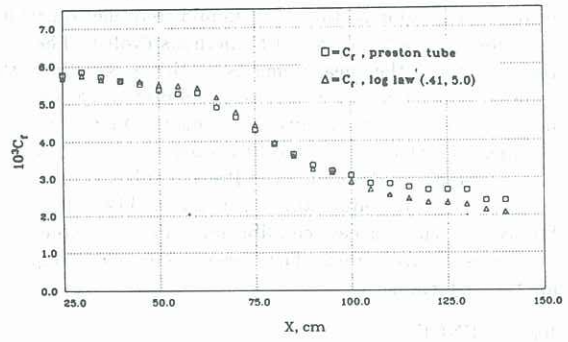

Figure 8. Preston tube and Clauser chart estimates of skin friction coefficient C_f with streamwise distance x.

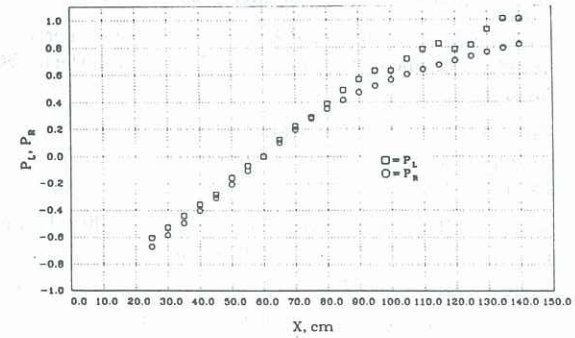

Figure 9. Momentum balance.

Spanwise Preston tube C_f measurements are within $\pm 2\frac{1}{2}\%$ over 40δ in the FPG at x=0.5m and over 20δ in APG at x=0.9m. Further downstream, at x=1.4m, the C_f variation is within $\pm 4\%$. The momentum balance shown in figure 9 is within 10%. These results indicate that the layer is acceptably two-dimensional.

Turbulence Quantities

Normal hot-wire data in the FPG (figure 10) show that trip effects decay rapidly in the near wall and outer regions but that longer development length is required for recovery in the the central region of the layer. However the the profiles have almost exactly the same shape over the last 20δ of the FPG region. The same behaviour is observed for the cross-wire data $\frac{\sqrt{-\overline{uv}}}{U_\infty}$, $\frac{\sqrt{\overline{v^2}}}{U_\infty}$ and $\frac{\sqrt{\overline{w^2}}}{U_\infty}$ but these are not shown here. This is further evidence that the layer is in a state of equilibrium before application of the APG.

Profiles of turbulence quantities in the APG region are shown with wall scaling in figures 11 (a) to (d). The close spacing (50mm) of the profiles provides a sensitive means of detecting inconsistencies in the data (assuming that the profiles should develop smoothly and monotonically with x). All the anomolies can be explained by uncertainties in U_τ of order 5%. Large values of all the fluctuating quantities in the central region of the layer emerge with streamwise distance. Note that $\frac{\overline{u^2}}{U_\tau^2}$ in the central region of the layer is larger than the peak value near the wall for $x >$ 1.5m. The same data has been plotted as $\frac{\sqrt{\overline{u^2}}}{U_0}$ versus $\frac{y}{\delta}$ in figure 12. For streamwise distances $x > 1m$ the absolute turbulence level remains very nearly constant and scales with $\frac{y}{\delta}$ in the outer half of the layer. Moreover the contours in figure 13 show that the absolute thickness of the region where $\frac{\sqrt{\overline{u^2}}}{U_0} < 0.06$ is nearly constant from near the end of the FPG region onwards. The same observation result is obtained for $\frac{\sqrt{-\overline{uv}}}{U_0}$, $\frac{\sqrt{\overline{v^2}}}{U_0}$ and $\frac{\sqrt{\overline{w^2}}}{U_0}$ but these data are not shown here.

CONCLUSIONS

Integration of total automated computer control into the experiment has provided data with a spatial density (31 profiles of mean flow and turbulence quantities so far) that would be daunting to obtain using conventional methods. Closely spaced profiles in the short region of FPG preceding the APG demonstrate that an equilibrium boundary layer has been established over about 20δ which is devoid of upstream trip effects. This is a suitable initial condition for

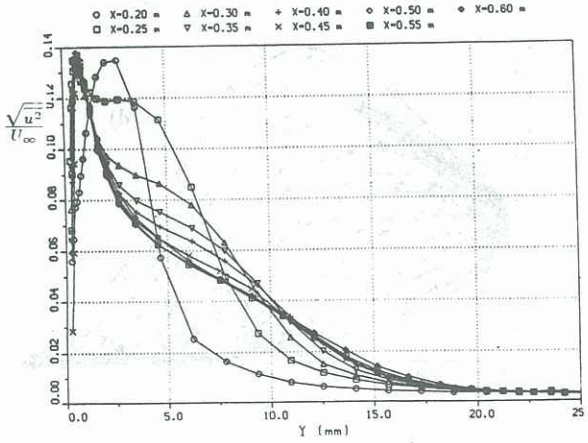

Figure 10. Development of streamwise turbulence component in FPG region.

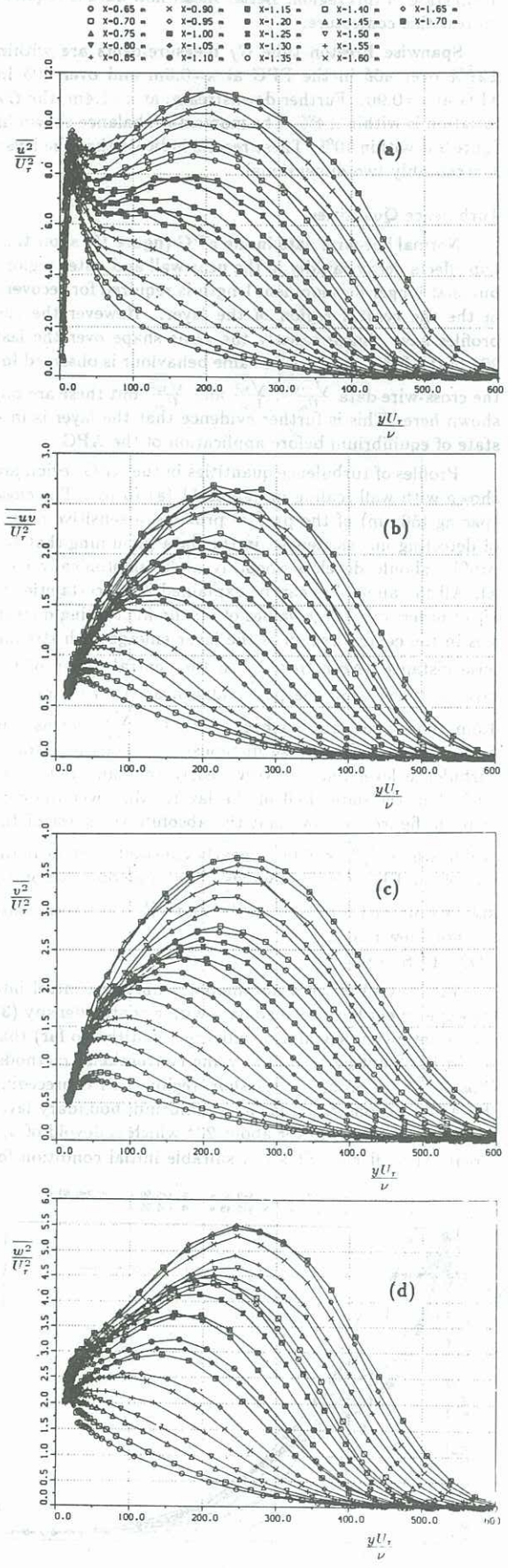

Figure 11. Streamwise development of Reynolds stresses in APG region. (a) $\frac{\overline{u^2}}{U_\tau^2}$ (b) $\frac{\overline{-uv}}{U_\tau^2}$ (c) $\frac{\overline{v^2}}{U_\tau^2}$ (d) $\frac{\overline{w^2}}{U_\tau^2}$

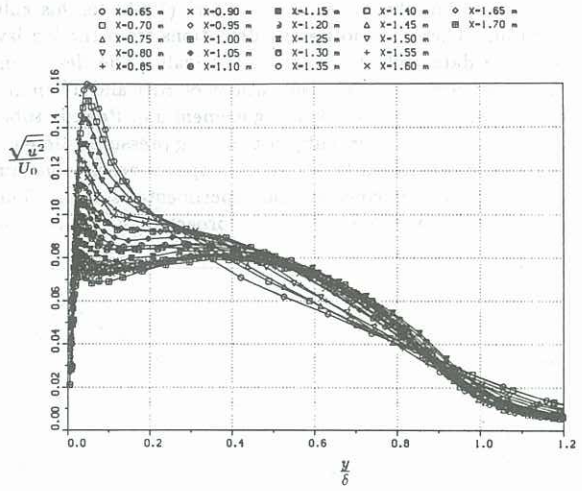

Figure 12. Streamwise development of $\frac{\sqrt{u^2}}{U_0}$

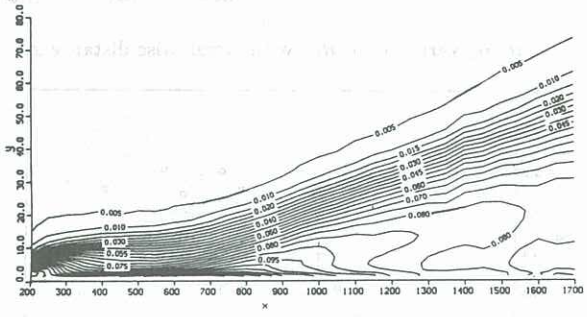

Figure 13. Contours of $\frac{\sqrt{u^2}}{U_0}$ throughout entire layer.

direct CFD simulations. A highly two-dimensional low Re_θ turbulent boundary layer then develops in the APG region. A large part of the layer is within the current capabilities of the simulations. However measurements are also obtained beyond this region so that they should continue to provide a challenging test flow as CFD methods evolve. The spatial density of the measurements in the APG allows the rapid growth to be followed closely and provides a sensitive means of judging the quality of the data. Much of the experimental scatter appears to be caused by uncertainties in C_f. A number of different sized Preston tubes will be used in an attempt to reduce this uncertainty. The layer could finally end up in a new equilibrium state (β_x =constant) but more accurate mean flow measurements are required for this determination.

REFERENCES

Hirt, F. and Thomann, H. (1986), "Measurement of wall shear stress in turbulent boundary layers subject to strong pressure gradients". J. Fluid Mech. **171:** 547- 562.

Jones, W.P. and Launder B.E. (1972), "Some properties of sink-flow turbulent boundary layers". J. Fluid Mech. **56:** 337-351.

Patel, V.C. (1965), "Calibration of Preston tube and limitations of its use in pressure gradients". J. Fluid Mech. **23:** 185-208.

Spalart, P.R. (1986), "Numerical study of sink-flow boundary layers". J. Fluid Mech. **172:** 307-328.

Spalart, P.R. (1988), "Direct simulation of a turbulent boundary layer up to Re_θ=1410. J. Fluid Mech. **187:** 61-98.